

Double Exchange in Electron Doped $\text{Ca}_{1-x}\text{Y}_x\text{MnO}_3$ Manganites

H. Aliaga, M. T. Causa, H. Salva, M. Tovar, A. Butera and B. Alascio.
Centro Atómico Bariloche and Instituto Balseiro
Comisión Nacional de Energía Atómica
8400 S.C. de Bariloche, Argentina.

D. Vega, G. Polla, G. Leyva, and P. Konig
Centro Atómico Constituyentes.
Comisión Nacional de Energía Atómica
Buenos Aires, Argentina.
(December 2, 2024)

We have studied magnetic and electric transport properties in the electron doped $\text{Y}_x\text{Ca}_{1-x}\text{MnO}_3$ manganite in the region $0 \leq x \leq 0.25$. We found an anomaly in the temperature dependence of the susceptibility curves for the low doped samples. With a simple model where antiferromagnetic (AF) superexchange and ferromagnetic double exchange (DE) interactions compete, we reproduce susceptibility vs temperature measurements. From the fitting parameters, we have found that DE interaction is about twice larger than the AF interaction. We conclude that the competition between DE and AF are the main driving forces that explains the magnetic, resistivity and magnetoresistivity properties found in low Y doped manganites.

PACS numbers: 75.30.Vn, 75.30.-m, 75.30.Et

I. INTRODUCTION

The existence of magnetoresistance (MR) in Mn oxides with perovskite structure was discovered at the very early stage of the study of the transition metal oxides¹. The interest in these oxides has revived recently due to the discovery of very large MR ($\sim 10^6\%$) which led to call this phenomenon as colossal magnetoresistance (CMR). At the same time the magnetic field induced insulator-metal and lattice-structural transition² was also discovered. Most studies were devoted to the perovskite compounds $\text{R}_x\text{A}_{1-x}\text{MnO}_3$ (R =trivalent rare earth and A =divalent alkaline earth) producing x Mn^{3+} and $(1-x)$ Mn^{4+} ions, respectively. Ferromagnetic (FM) double-exchange interaction between localized t_{2g} Mn electron configuration, mediated by itinerant spin-polarized e_g electrons, is in the base of CMR. The concentration x is not the only parameter to be taken into account in CMR materials. Chemical parameters as the average R-A cationic radius and the cationic size mismatch quantified by the variance σ^2 of the ionic radii^{3,4} are also relevant. The phase diagrams for $\text{R}_x\text{A}_{1-x}\text{MnO}_3$ families were found to be non-symmetric and hole or electron doping cause disimilar effects. Theoretical studies⁵ suggested at least three possible scenarios to understand the low doping region: i) Canting of the magnetic structure. ii) Phase separation into ferromagnetic and anti-ferromagnetic phases and charge separation. iii) Ferromagnetic polarons. Therefore, experiments on families of compounds, covering different ranges of physical and chemical parameters can be used to clarify this issue. In this paper we study structural, resistivity and magnetic properties of $\text{Ca}_{1-x}\text{Y}_x\text{MnO}_3$. Trivalent Y is one of the smallest ions sintetizing in the perovskite structure. Fur-

ther, the non magnetic character of Y allow the study of the dc magnetic susceptibility (χ) in the paramagnetic (PM) phase without interference from other magnetic species. We have sintered single orthorhombic phases⁶ for $x < 0.8$ and we have measured resistance and magnetoresistance in the region $0 \leq x \leq 0.25$, confirming the presence of DE mechanism⁷. We present here magnetic and resistivity measurements in the region $0 \leq x \leq 0.25$. We analyse these measurements in the PM and ordered phases to show that they can be understood in terms of small magnetic polarons⁸ arising from the DE mechanism between Mn^{3+} and Mn^{4+} .

II. EXPERIMENTAL

Ceramic polycrystalline samples of $\text{Ca}_{1-x}\text{Y}_x\text{MnO}_3$ were prepared by solid state reaction methods.^{6,7} Room temperature x-rays diffractograms show that CaMnO_3 crystallizes in an orthorhombic P_{nma} cell with parameters $a=5.284(5)\text{\AA}$, $b=7.453(5)\text{\AA}$, and $c=5.266(5)\text{\AA}$. For $x \leq 0.25$ single phase material was obtained with O structure. Electrical resistivity was measured with the 4-probe method using a current source of $10\mu\text{A}$ or $100\mu\text{A}$ (according to the magnitud of resistivity). The demagnetization M was measured with a SQUID magnetometer between 5K and 300K and $H \leq 50\text{kOe}$ and with a Faraday Balance magnetometer between 300K and 1000K with $H \leq 10\text{kOe}$. The ratio M/H was found independent of H for $T \geq 140\text{K}$.

III. RESULTS

In Fig. 1 we show measured H/M vs. T (open symbols) for the samples $x=0, 0.05, 0.07$ and 0.10 . As discussed in¹⁶, the Van Vleck contribution is expected for Mn^{4+} ions. In our measurements this contribution was subtracted, in the paramagnetic phase, proportionally to $(1-x)$.

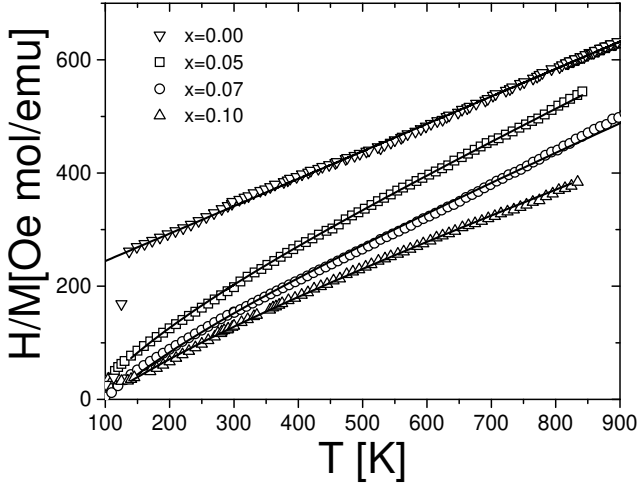


FIG. 1. Measured $\chi^{-1}(T)$ curves (open symbols) with $H=10$ kOe and calculated (lines) for the samples $x=0, 0.05, 0.07$ and 0.10 . Notice the deviation from the Curie law, starting at $\simeq 350$ K. M vs. H curves show linear dependence for $T \geq 140$ K.

The $CaYMnO_3$ data were fitted with a Curie Weiss law $\chi^{-1}=C/(T - \Theta)$, where C is the Curie constant and Θ is the Curie-Weiss temperature, obtaining $C=(1.8\pm 0.1)$ emuK/mol (near the expected Mn^{4+} value 1.875) and $\Theta \approx 400$ K. These values points to a strong antiferromagnetic superexchange interaction between Mn^{4+} ions. Using neutron diffraction at temperatures below the magnetic order temperature, Wollan and Kohler¹⁰ found G-type AF magnetic order ($T_N \sim 120$ K). Further magnetic measurements have shown the existence of a weak ferromagnetic moment (WFM)¹¹ below T_N of about $M_{WFM} \sim 0.03\mu_B/Mn$ ion.

For the samples $x=0.05, 0.07$ and 0.10 , the χ^{-1} curves deviate substantially from the Curie Law at $T \lesssim 350$ K. We have obtained from high temperature fits ($T > 400$ K) the values $\Theta=-60, +40$ and $+50$ for the samples $x=0.05, 0.07$ and 0.10 , respectively. Small Y doping causes large changes in the Θ values, indicating an evolution from a strong antiferromagnetic system for $x=0$ to a FM one for $x \approx 0.10$.

In Fig. 2 we show M vs. T curves measured with $H=5$ kOe, for some selected samples. Broad magnetic order temperatures of about ~ 115 K can be observed. In more detail, we show in the inset of Fig. 2 the magnetic transition temperatures T_{mo} , defined as the maximum in

$|dM/dT|$. For $0 \leq x \leq 0.06$, T_{mo} vs. x decreases, and in the range $0.06 \leq x \leq 0.25$, T_{mo} vs. x increases. For $x=0$ the ratio $\Theta/T_N \sim 4$. This is an indication of the importance of second neighbors interaction.¹⁶

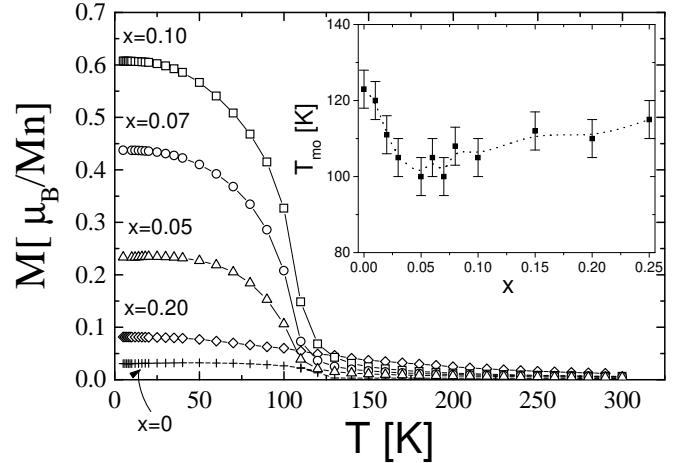


FIG. 2. M vs. T curves for same selected samples with $H=5$ kOe applied. In the Inset: magnetic order temperatures as function of x , extracted from M vs. T curves. Solid lines are guides to the eyes.

In Fig. 3 we show the M vs. H at $T=5$ K for some selected samples. For $H \gtrsim 30$ kOe, $M(H)$ can be approximated by: $M = M_0 + \chi_{AF} H$, where M_0 is the ferromagnetic contribution to M , and χ_{AF} is the antiferromagnetic susceptibility. Note that M_0 is much smaller than the expected for full FM alignment ($M_S \sim 3-3.25\mu_B/Mn$ ion).

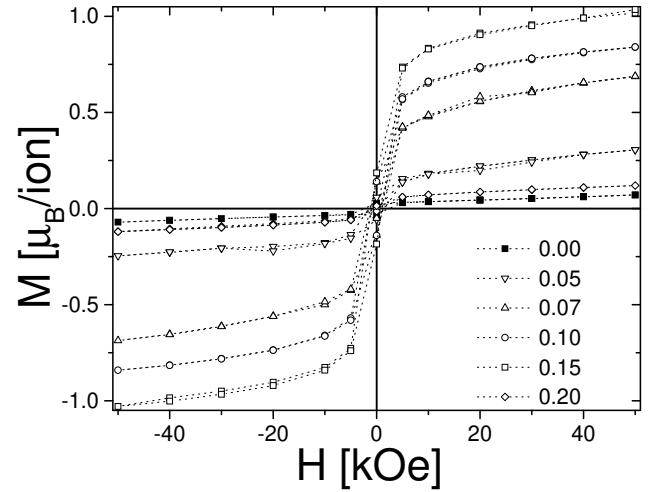


FIG. 3. M vs. H curves at $T=5$ K for same selected samples. Magnetic saturation is not reached in any case ($M_0 \sim 3\mu_B$). Dotted lines are guides to the eyes.

For $H \lesssim 10$ kOe, $M(H)$ raises more rapidly than in the

high field regime. The remanent magnetization, M_R is low compared with a typical FM and almost independent of x . In Fig. 4(a) we plotted M_0 vs. x , a strong development of the magnetic moment in the region $0 \leq x \leq 0.15$ and a sharp decrease in the range $0.15 < x \leq 0.25$ can be seen. In the region $0 < x \leq 0.05$, $M_0(x)$ starts with a slope of $\sim 0.85\mu_B/\text{Mn ion}$ and shows concavity. In the region $0.05 < x \leq 0.15$ this curve displays convexity and has an average slope of $\sim 6.4\mu_B/\text{Mn ion}$. Further, in the region $0.15 \leq x \leq 0.25$, the M_0 decreases sharply with the concentration x . These results are in agreement with Refs.^{12–14}. In Fig. 4(b) we present the concentration dependence of the electric resistivity⁷ ρ measured at 100K. We can see that the resistivity decreases 5 orders of magnitude in the range $0 \leq x \leq 0.05$, stays in the same order of magnitude in $0.05 \leq x \leq 0.15$ and then increases 3 orders of magnitude in range $0.15 \leq x \leq 0.25$. Comparing Figs. 4(a) and 4(b) in the range $0 \leq x \leq 0.15$, we see that the greater the concentration of carriers, the greater the conductivity and the magnetic moment. These results are in qualitatively agreement¹⁵ with the DE mechanism. In the region $0.15 \leq x \leq 0.25$ the resistivity increases and the magnetic moment decreases, the DE mechanism is broken, leading to a low magnetic moment-insulator state.

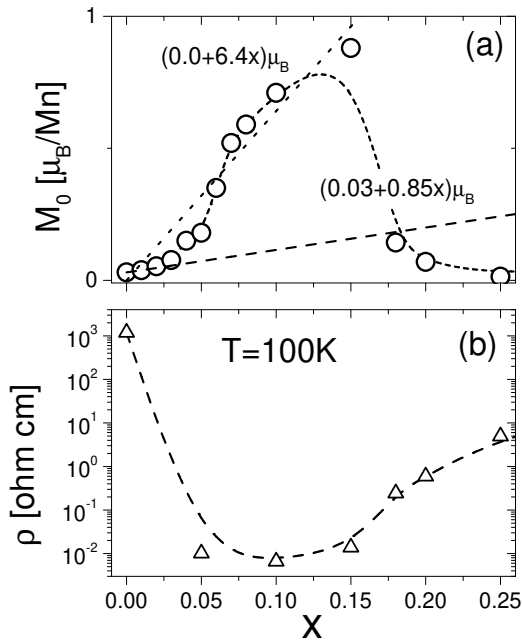


FIG. 4. (a) M_0 vs. x , straight line is a linear fit for $0 \leq x \leq 0.15$. (b) ρ vs. x , at $T=100\text{K}$ and no magnetic field applied. Notice the strong correlations between magnetism and resistivity. Dotted lines are only guides to the eye.

IV. DISCUSSIONS

As Y^{3+} is added in the AF pure sample CaMnO_3 , itinerants e_g electrons are introduced in the system. These

e_g electrons polarize the AF background⁸ surrounding each Mn^{3+} spin, forming magnetic polarons. This hypothesis is supported from two facts: 1) the low remanent magnetization, and 2) the two regimes we found in the M vs. H curves. Within this model the large increase in M with H for $|H| \leq 10\text{kOe}$ at low temperatures is mainly due to the alignment of these small magnetic polarons with H . For $|H| \gtrsim 10\text{kOe}$, the further increase of magnetization with field is due to the antiferromagnetic susceptibility of the background. In the very diluted region $x \sim 0$, we expect that Jahn-Teller distortions surrounding each Mn^{3+} localize the e_g electrons, forming a combined lattice-magnetic polaron. In this regime each Mn^{3+} added has an extra $S=1/2$ e_g electron, that polarizes with magnetic fields of $\sim 10\text{kOe}$, expecting $M_0 = [1\mu_B/\text{Mn-ion}]x$ (see Fig. 4a).

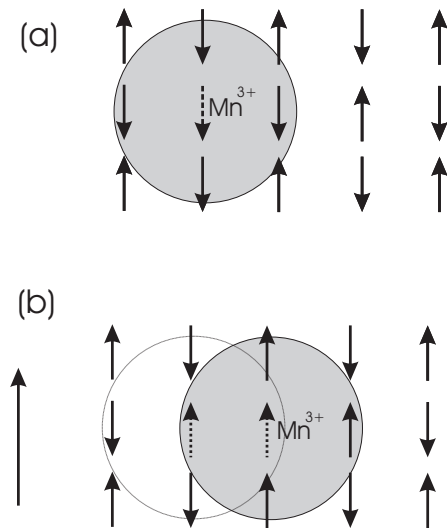


FIG. 5. (a) A Mn^{3+} that replaces a Mn^{4+} , couples ferromagnetically with the Mn^{4+} neighbors, after a spin flip process. (b) With an applied H , the e_g electrons of the misaligned Mn^{3+} spins hop to a Mn^{4+} neighbor, with the $S = 3/2$ spin aligned with H , after two spin-flip processes.

In the region $0.01 \leq x \leq 0.05$ these polarons interact with each other, so the M_0 vs x curve displays concavity. The magnetic order temperature T_{mo} decreases because the bonds of the AF interactions between Mn^{4+} are weakened by the DE interaction between Mn^{4+} and Mn^{3+} spins. The resistivity in this region drops sharply possibly due to some canting of the AF background, allowing the excitation of the e_g electrons from the localized Jahn-Teller states to a narrow conduction band. In the region $0.05 \leq x \leq 0.15$, we find $M_0 \sim [6.4\mu_B/\text{Mn-ion}]x$, indicating that the polarons have larger magnetic moment. The magnetic order temperature T_{mo} increases due to the strengthening of the FM order induced by the DE mechanism. In this region, the resistivity stands in the same order of magnitude, and maximum magnetoresistance was measured⁷. We can understand the results in the region $0.05 \leq x \leq 0.15$ with the following model: each

Mn^{3+} that replaces a Mn^{4+} , couples ferromagnetically with the Mn^{4+} neighbors, after a spin flip process (see Fig. 5a). This ferromagnetic coupling allows the kinetic energy gain due to the hopping of the e_g electron into the neighboring localized spins, forming a magnetic polaron, comprising the Mn^{3+} site and its nearest neighbors. With zero applied field these Mn^{3+} spins, with excess $M = 4\mu_B$ magnetic moment, orient in random up-down directions in the lattice. When a magnetic field H is applied, the e_g electrons of these misaligned Mn^{3+} spins hop to a Mn^{4+} neighbor, with its $S = 3/2$ spin aligned with H , after two spin-flip processes (see Fig. 5b). $M_0 = [7\mu_B/\text{Mn-ion}]x$ is expected for this case. Turning to the paramagnetic phase, the most peculiar feature observed is the deviation from the Curie-Weiss law, presenting a negative curvature of the $\chi^{-1}(T)$ curves (Fig. 1). To propose a framework for the understanding this behaviour, we considered that the magnetically ordered state has two sublattices a and b . In both sublattices there are randomly distributed Mn^{4+} and Mn^{3+} ions with concentrations $(1-x)$ and x , respectively. We consider exchange interactions with first and second neighbors, between Mn^{4+} - Mn^{4+} , Mn^{3+} - Mn^{3+} and Mn^{4+} - Mn^{3+} pairs. The equations to be satisfied for the magnetization M in the mean field approximation are:

$$M_4^a T = C_4 (H + \gamma_4 (1-x) M_4^b + \gamma'_4 (1-x) M_4^a + \gamma x M_3^b + \gamma' x M_3^a) \quad (1)$$

$$M_4^b T = C_4 (H + \gamma_4 (1-x) M_4^a + \gamma'_4 (1-x) M_4^b + \gamma x M_3^a + \gamma' x M_3^b) \quad (2)$$

$$M_3^a T = C_3 (H + \gamma_3 x M_3^b + \gamma'_3 x M_3^a + \gamma x M_4^b + \gamma' (1-x) M_4^a) \quad (3)$$

$$M_3^b T = C_3 (H + \gamma_3 x M_3^a + \gamma'_3 x M_3^b + \gamma x M_4^a + \gamma' (1-x) M_4^b) \quad (4)$$

where superindexes 4 and 3 indicate Mn^{4+} and Mn^{3+} ions respectively, subindexes a y b correspond to the two different sublattices, $1-x$ and x are the concentrations of Mn^{4+} and Mn^{3+} respectively; C_4 and C_3 are the Curie constants, γ_4 and γ'_4 are the parameters for magnetic coupling between first and second neighbors Mn^{4+} ions, γ_3 and γ'_3 indicate coupling between first and second Mn^{3+} neighbors and γ and γ' are the coupling parameters between first and second Mn^{4+} and Mn^{3+} neighbors. Notice that γ -parameters have no units, for example in the case of $x = 1$, $\Theta = C_4(\gamma_4 + \gamma'_4)$. Solving these set of equations, the total magnetization can be calculated as:

$$M = \frac{1}{2} ((M_4^a + M_4^b)(1-x) + (M_3^a + M_3^b)x) \quad (5)$$

The total magnetic susceptibility is $\chi = M/H$. Data best fits are shown in Fig. 1, where a good agreement

between measurements and calculations can be observed. Only three independent parameters ($\gamma_4 + \gamma'_4$, $\gamma_3 + \gamma'_3$ and $\gamma + \gamma'$) are necessary to fit the experimental curves in the paramagnetic zone.

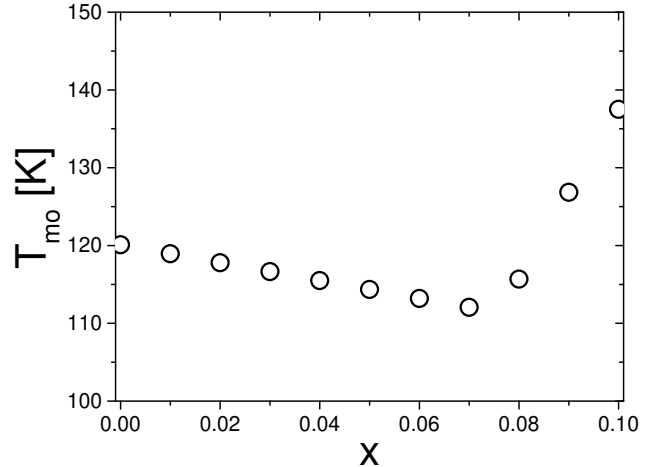


FIG. 6. Magnetic order temperatures vs doping x , calculated for $\gamma_4 = -132$, $\gamma'_4 = -71$, $\gamma_3 = \gamma'_3 = 0$, $\gamma = 190$ and $\gamma' = 160$.

We fitted the $x=0$ curve with $\gamma_4 + \gamma'_4 = -203$. The $x=0$ sample has $\Theta = -397$ K and $T_N \sim 120$ K as characteristic temperatures. In order to obtain these values, we fixed: $\gamma_4 = -132$, $\gamma'_4 = -71$. For $0 \leq x \leq 0.05$, we see that the contribution to the total magnetization of the Mn^{3+} spins is quite small compared to the contribution of the Mn^{4+} species. For this reason we expect great indeterminacy in the γ_3 and γ'_3 parameters, so we have fixed them following the cases: *i*) neglect it: $\gamma_3 + \gamma'_3 = 0$; *ii*) suppose equal to the interaction between Mn^{4+} : $\gamma_3 + \gamma'_3 = -203$ and *iii*) taking the parameter $\gamma_3 + \gamma'_3$ from the Θ measured in $LaMnO_3$.¹⁶ In the high temperature regime, $LaMnO_3$ presents pseudocubic phase with $\Theta = 220$ K, giving $\gamma_3 + \gamma'_3 = 73$ (ferromagnetic exchange interaction between Mn^{3+} spins). Despite of the case considered, the $\gamma + \gamma'$ -values found are nearly the same ($\pm 10\%$). In Table I there is a summary of the $\gamma + \gamma'$ -parameter that fit the curves $\chi^{-1}(T)$ according to case *i*). The $\gamma + \gamma'$ parameter obtained are always positive and approximately two times larger than $\gamma_4 + \gamma'_4$, denoting strong ferromagnetic coupling between Mn^{4+} and Mn^{3+} pairs. Solving the equations 1-4 we obtain four solutions, where the largest T correspond to T_{mo} plotted in the Inset of Fig. 2. In Fig. 6 we plot the calculated T_{mo} , for $\gamma_3 = \gamma'_3 = 0$, $\gamma = 190$ and $\gamma' = 160$ (the average value of considered case *i*) is $\gamma + \gamma' = 350$). In the range $0 \leq x \leq 0.07$, we obtained that T_{mo} decreases linearly from 120 K to 112 K, the magnetic order corresponds to AF interaction between Mn^{4+} - Mn^{4+} and Mn^{3+} - Mn^{3+} pairs, but FM between Mn^{4+} - Mn^{3+} pairs. For $0.08 \leq x \leq 0.10$, the calculated T_{mo} increases linearly from 115 K to 137 K and corresponds to

full FM alignment. We obtained good agreement between calculated and measured T_{mo} . In the region $0.08 \leq x \leq 0.10$, the calculated T_{mo} increases sharper than the measured one. This disagreement could be interpreted in terms of others interactions that start to play (charge ordering insulator state, chemical disorder introduced by Yttrium cations, etc) and for the fact that this region could be out of the dilute limit of the present model ($x \ll 1$).

x	$\gamma + \gamma'$
0.05	361
0.07	386
0.10	310

Table I: Parameter $\gamma + \gamma'$ obtained for case i) (see text) as function of concentration x. The $-\gamma + \gamma'$ parameter is a measurement of the magnetic interaction between Mn^{3+} and Mn^{4+} spins. The $-\gamma + \gamma'$ values obtained are approximately twice larger than the Mn^{4+} - Mn^{4+} magnetic interactions, and positive, indicating strong FM coupling between Mn^{4+} - Mn^{3+} pairs.

V. CONCLUSIONS

We have measured structural, magnetic and resistivity properties as function of temperature and magnetic field in the manganites $Ca_{1-x}Y_xMnO_3$, in the region $0 \leq x \leq 0.25$. Despite of the small cationic size of Yttrium, and the large cationic mismatch between Yttrium and Calcium, we have synthesized single phase with orthorrombic structure for this doping. Strong correlation between magnetization and conductivity in the region $0 \leq x \leq 0.15$ was found, allowing to conclude that DE mechanism is present in this compound. We have measured magnetic and transport properties that are in good agreement¹²⁻¹⁴ with studies on other family of compounds in the electron doping regime. These properties are weakly dependent on the cationic species used to synthesize the structure. The magnetic order temperatures decreases from 120K to 100K in the region $0 \leq x \leq 0.06$ due to the weakening of the AF background by lattice-magnetic polarons and then increases from 100K to 115K in the range $0.06 \leq x \leq 0.15$ due to the strengthening of a DE FM phase. In the samples $x=0.05$, 0.07 and 0.10 , the $\chi^{-1}(T)$ curves deviate substantially from the Curie Law at $T \lesssim 300K$, showing strong ferromagnetic correlations (though there is linear dependence of M vs H for $T \geq 140K$). We also have found from M vs. H curves at $T = 5K$ and $H = 50kOe$ a maximum magnetic moment of $\sim 1\mu_B$, that is far from saturation ($M_0 \sim 3\mu_B$). The magnetization M increases sharply in the region $0 \leq |H| \leq 10kOe$, and more moderately in the region $10kOe \leq |H| \leq 50kOe$. In the first case, we propose that the low field response is due to the displacement of the e_g electrons from one magnetic lattice into the other, forming lattice-magnetic polarons (Fig. 5). In the second case the magnetic response to the field is mainly due to the canting of the AF background. We

proposed a mean field model where FM and AF interactions between Mn^{3+} and Mn^{4+} spins compete and fitted $\chi^{-1}(T)$ curves for $x = 0.05$, 0.07 and 0.10 . Extracting parameters from this model, we conclude, the FM Double Exchange interactions are about twice the magnitud of the AF interaction. We calculated T_{mo} with the parameters extracted from the model. This temperatures are in good agreement with the measured one. We can understand within this model that measured T_{mo} in the region of doping $0 \leq x \leq 0.06$ decreases due to the weakening of the AF background by the FM DE interaction between Mn^{4+} - Mn^{3+} pairs. In the region $0.06 \leq x \leq 0.15$ increases due to the strengthening of the DE FM state.

Acknowledgements : We acknowledge partial support from ANPCYT (Argentina)-PICT 3-52-1027. H. A. is CONICET (Argentina) PhD-fellow.

¹ C. W. Searle and S. T. Wang, Can. J. Phys. **47**, 2023 (1969).

² Y. Tokura and Y. Tomioka, J. Mag. Mag. Mat. **200**, 1 (1999).

³ L. M. Rodríguez-Martínez and J. P. Attfield, Phys. Rev B **54**, R15622 (1996).

⁴ C. Martin, A. Maignan and M. Hervieu, B. Raveau, Phys. Rev B **60**, 12191 (1999).

⁵ E. Dagotto, S. Yunoki, A. L. Malvezzi, A. Moreo, J. Hu, S. Capponi, D. Poilblanc, N. Furukawa, Phys. Rev. B, **58**, 6414 (1998).

⁶ D. Vega, G. Leyva, G. Polla, P. Konig, H. Lanza, A. Esteban, H. Aliaga, M. T. Causa, M. Tovar and B. Alascio, J. Solid State Chem. (accepted).

⁷ H. Aliaga, M. T. Causa, B. Alascio, H. Salva, M. Tovar, D. Vega, G. Polla, G. Leyva and P. Konig, J. Mag. Mag. Mat. (accepted).

⁸ C. D. Batista, J. Eroles, M. Avignon and B. Alascio, Phys. Rev. B **58**, R14689 (1998).

⁹ M. E. Lines, Phys. Rev. **164**, 736 (1967).

¹⁰ E. O. Wollan and W. C. Kohler, Phys. Rev. **100**, 545 (1955).

¹¹ G. H. Jonker, Physica **22**, 707 (1956); V. M. Yudin, A. I. Gavrilishina, M. V. Artemeva and M. F. Bryshina, Sov. Phys. Solid State **7**, 8 (1966).

¹² A. Maignan, C. Martin, F. Damay and B. Raveau, Chem. Mater. **10**, 950 (1998).

¹³ I. O. Troyanchuk, H. Szymczak and A. Nabialek, J. Solid State Chem. **131**, 144 (1997).

¹⁴ J. J. Neumeier and J. L. Cohn, Phys. Rev. B, **61**, 21, 14319 (2000).

¹⁵ C. Zener, Phys. Rev. **82**, 403 (1951); P. W. Anderson and H. Hasegawa, Phys. Rev. **100**, 675 (1955).

¹⁶ D. L. Huber, A. Alejandro, A. Caneiro, M. T. Causa, F. Prado, M. Tovar and S. B. Oseroff, Phys. Rev. B **60**, 12155 (1999).